ACS Catalysis

RESEARCH ARTICLE

pubs.acs.org/acscatalysis

Study of the Properties of $CuO/VO_x/Ti_{0.5}Sn_{0.5}O_2$ Catalysts and Their Activities in NO + CO Reaction

Lihui Dong,[†] Lingling Zhang,[†] Chuanzhi Sun,[†] Wujiang Yu,[†] Jie Zhu,[†] Lianjun Liu,[†] Bin Liu,[†] Yuhai Hu,[†] Fei Gao,*[,‡] Lin Dong,*[,†,‡] and Yi Chen[†]

[†]Key Laboratory of Mesoscopic Chemistry of MOE, School of Chemistry and Chemical Engineering and [‡]Center of Modern Analysis, Nanjing University, Nanjing, 210093, P. R. China

ABSTRACT: $CuO/VO_x/Ti_{0.5}Sn_{0.5}O_2$ catalysts were prepared by an impregnation method and were tested on a NO + CO model reaction. Both copper oxide and vanadium oxide can be highly dispersed on $Ti_{0.5}Sn_{0.5}O_2$ (denoted as TS, hereafter) support. The dispersed oxides form V−O−Cu species when coexisting in the catalyst system. The formation of V−O−Cu species renders the dispersed vanadium oxide aggregated and easier to be reduced; in contrast, the reduction temperature of dispersed copper oxide species is evidently higher than that without vanadium oxide (CuO/TS samples). The surface dispersed V−O−Cu species are mainly the active component for the NO + CO reaction. The activities of CuO/VO_x/TS catalysts are highly dependent on the operating temperature and the amount of V−O−Cu species. In the reaction atmosphere, NO molecules are adsorbed onto Cu^{2+} sites, reduced V^{x+} (V^{4+} or V^{3+}) sites, and even TS support, forming −NO and NO_3^- species. Adsorption of CO molecules proceeds only on Cu^+ sites. The active species change with varying reaction temperature; hence, the NO + CO reaction goes through different mechanisms at low and high temperatures over these catalysts.

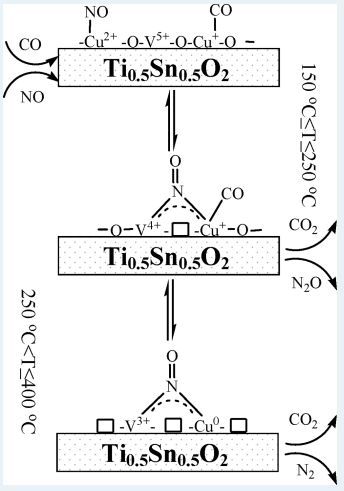

KEYWORDS: copper oxide, vanadium oxide, $Ti_{0.5}Sn_{0.5}O_2$ mixed oxide, V−O−Cu species, NO + CO reaction, in situ FT-IR

1. INTRODUCTION

Mitigation of NO_x from the stationary and moving sources, such as a coal-burning plant and automotive exhaust emissions, etc., has been one of the key subjects in catalysis. This problem has been solved scientifically and technically as a result of the invention of three-way catalysts (TWC),[1−11] but economically, the challenge still exists because of the high cost of such catalysts (noble metals are need).[5−11] Because of that high cost, developing highly efficient noble-metal-free catalysts is one of the primary focuses in current deNO_x research.

In past decades, much effort has been made to develop copper oxide-based catalysts because of their promising applications in related reactions. Generally, copper oxide (no doping species) supported on metal oxides is of low activity and unstable. Therefore, the research has been focused mainly on coupling copper oxide with other metals/metal oxides over various kinds of supports.[12−17] Shelef et al.[13] studied the activities of $CuO−CrO_3/Al_2O_3−SiO_2$ catalysts in the NO + CO reaction and suggested that in the reaction atmosphere, the formation of lower valence copper oxide and chromium oxide species in the catalysts is positive to the reaction. Panayotov et al.[14,15] developed $CuO−MO_x/\gamma$-Al_2O_3 (M = Co, Mn) catalysts and tested them in the same reaction. The activities of the catalysts increase with the amount of (Cu + M) species. Jiang et al.[16] investigated the influence of ZrO_2 addition on the activities of CuO/TiO_2 catalysts in the NO + CO reaction and concluded that the strong interaction between CuO and ZrO_2 improves the performance of the catalysts. Recently, we have studied $CuO−CoO_x$ (or MnO_x)/$Ce_{0.67}Zr_{0.33}O_2$ catalysts and found that the binary metal oxides are the active species in the NO + CO reaction; that is, the strong interaction between CuO and CoO_x (or MnO_x) improves the activity of the catalysts.[17,18] These studies, to some extent, improve the performance of copper oxide species, but they also unambiguously indicate that the catalyst systems are very complicated. Further study is still needed for the catalysts.

Vanadium oxide-based catalysts are well known for their high efficiency in oxidation reactions, for example, the oxidation of sulfur dioxide, carbon monoxide, and hydrocarbons.[19−21] Vanadium oxide supported on TiO_2 was found to exhibit superior activities in selective catalytic reduction of NO_x by NH_3.[22,23] Recently, $TiO_2−SnO_2$ mixed oxide has received rapidly increasing attention.[24,25] TiO_2 and SnO_2 more easily form rutile solid solutions that possess larger surface areas at high temperatures, and therefore, the mixed oxides have potential application in the development of metal oxide supported catalysts. All these draw our interest toward designing effective CuO/VO_x/TS catalysts that may be applied to the NO + CO reaction.

In this study, TS mixed oxide with high surface area was synthesized for the support of CuO/VO_x/TS catalysts. Attention has been paid to (1) the dispersion and reduction of copper oxide and vanadium oxide on TS support, (2) the activities of

Received: January 28, 2011
Revised: March 16, 2011
Published: March 21, 2011

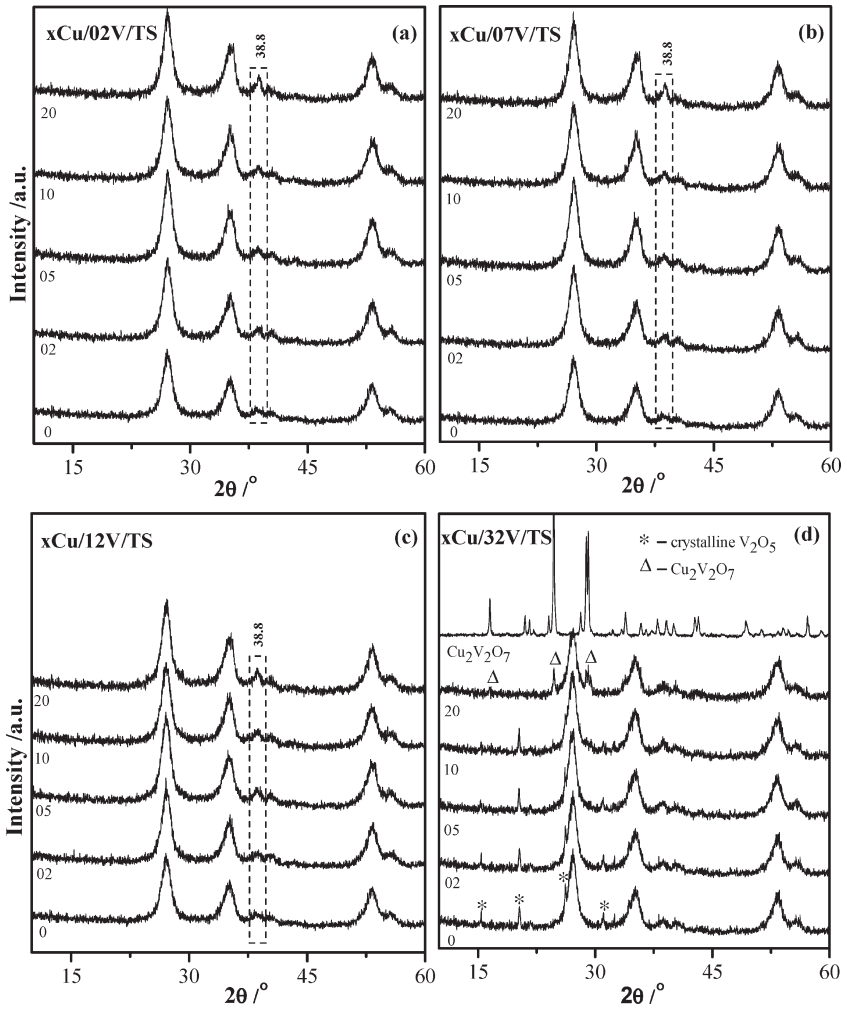

Figure 1. XRD patterns of (a) *x* Cu/02 V/TS; (b) *x* Cu/07 V/TS; (c) *x* Cu/12 V/TS and (d) *x* Cu/32 V/TS samples (*x* = 0, 02, 05, 10, 20).

CuO/VO_x/TS catalysts in NO + CO reaction, and (3) how NO and CO molecules interact with CuO/VO_x/TS and active species at low and high reaction temperatures.

2. EXPERIMENTS

2.1. Preparation of Catalysts. $Ti_{0.5}Sn_{0.5}O_2$ (rutile structure) mixed oxide was synthesized by a coprecipitation method. An aqueous solution containing requisite amounts of $TiCl_4$ and $SnCl_4$ (molar ratio of Ti/Sn = 1:1) was precipitated by ammonium hydroxide solution (25% ammonia) under vigorous stirring. The resultant hydroxide precipitation was dried at 110 °C for 12 h and then calcined at 550 °C for 4 h in flowing air. The surface area of TS is 88 $m^2 \cdot g^{-1}$, which was determined via nitrogen adsorption at 77 K with the Brunauer−Emmett−Teller (BET) method using a Micromeritics ASAP-2020 adsorption apparatus.

x CuO/TS samples were prepared by wet impregnating TS support with an aqueous solution containing a requisite amount of $Cu(NO_3)_2$. The samples were dried at 110 °C for 12 h and then calcined at 450 °C for 4 h in flowing air. The resultant *x* CuO/TS samples were denoted as *x* Cu/TS.

VO_x/TS samples were prepared by wet impregnation of TS support with an aqueous solution of NH_4VO_3. Oxalic acid was added to the solution (molar ratio of NH_4VO_3/oxalic acid = 1:2) to render full dissolution of ammonium metavanadate precursor. The NH_4VO_3/TS samples were dried overnight at 110 °C and calcined at 500 °C for 4 h in flowing air. The resultant VO_x/TS samples were denoted as V/TS.

Samples with copper oxide supported on V/TS were prepared by impregnating the V/TS supports with an aqueous solution containing a requisite amount of $Cu(NO_3)_2$. The samples were dried at 110 °C for 12 h and then calcined at 450 °C for 4 h in flowing air. The loading amount of copper oxide was calculated by referring to the original surface area of TS in the V/TS samples. For simplicity, CuO/V/TS samples were denoted as *x* Cu/*y* V/TS, e.g., 10 Cu/12 V/TS, corresponding to a sample with the loading amounts of copper oxide and vanadium oxide being 1.0 mmol Cu/100 m^2 TS and 1.2 mmol V/100 m^2 TS.

2.2. Characterization. X-ray powder diffraction (XRD) patterns were collected on a Philips X'pert Pro diffractometer using Ni-filtered Cu Kα radiation (λ = 0.154 18 nm). The X-ray tube was operated at 40 kV and 40 mA. Laser Raman spectra (LRS) were recorded by using a Renishaw Invia Raman spectrometer. Raman excitation at 514.5 nm was provided by an Ar^+ laser. Raman spectra were obtained by coadding 3 scans of 20 s at 4 cm^{-1} resolution and 20 mW laser power under ambient conditions. Infrared spectra (IR) were measured on a Nicolet

dx.doi.org/10.1021/cs200045f |*ACS Catal.* 2011, 1, 468–480

5700 FT-IR spectrometer at a 4 cm^{-1} resolution. Samples were pressed into a KBr pellet. For in situ spectra following CO and NO adsorption, self-supporting wafers (≈ 10 mg) of the samples were prepared and were mounted inside a purpose-made airtight IR cell, which could be heated up to 350 °C. Before each adsorption experiment, the sample was pretreated in a flowing N_2 stream (50 mL·min^{-1}) at 100 °C for 1 h to remove impurities and then cooled down to room temperature in the N_2 atmosphere. At room temperature, the sample wafers were exposed to a stream of CO−Ar (10% of CO by volume) or NO−Ar mixture (5% of NO by volume) at a flow rate of 5 mL·min^{-1} for 30 min. Then, the cell was heated at a rate of 10 °C·min^{-1}, and IR spectroscopy was recorded for the sample at a desired temperature. Temperature-programmed reduction (TPR) was carried out in a quartz U-tube reactor. A 50-mg sample was used for each measurement. Before being switched to H_2−Ar mixture (7% H_2 by volume), the sample was pretreated in a N_2 stream at 100 °C for 1 h and was then cooled down to room temperature. The temperature was increased linearly at a rate of 10 °C·min^{-1}. A thermal conductivity detector was used for tail gas analysis. Electron paramagnetic resonance (EPR) spectra were recorded on a Bruker EMX spectrometer using a 100-kHz modulation and a 4-G standard modulation width. The spectra were recorded at room temperature. X-ray photoelectron spectroscopy (XPS) analysis was performed on a PHI 5000 Versaprobe system using monochromatic Al Kα radiation (1486.6 eV). All binding energies were referenced to the C 1s peak at 285.0 eV. The elements (O, Cu, V, Ti, and Sn) were detected by means of XPS.

2.3. NO + CO Reaction. The NO + CO reaction was carried out on a homemade micro reactor. Before reaction, the samples were pretreated in a N_2 stream (50 mL·min^{-1}) at 100 °C for 1 h to remove the impurities and were then cooled down to room temperature in a N_2 atmosphere. The reaction gas was composed of 5% NO, 10% CO, and 85% He by volume. A 25-mg sample was used for each test at a gas space velocity of 24 000 mL·$g^{-1}h^{-1}$. The reaction products were analyzed using a thermal conductivity detector. N_2, NO and CO were separated by a 13X molecular sieve packed column; CO_2 and N_2O were separated by a Porapak Q packed column.

3. RESULTS AND DISCUSSION

3.1. XRD Results. Figure 1 shows XRD patterns of various *x* Cu/*y* V/TS samples. For *x* Cu/TS samples, only the diffraction peaks of TS support are observed. Hence, for brevity, the patterns are not shown. The diffraction peaks of CuO (typically at 2θ = 35.5 and 38.7°) significantly overlap with those of *y* V/TS support, rendering it difficult to determine the dispersion capacity of copper oxide. Nonetheless, the patterns still present some notable features that are related to the loading amounts of copper oxide and vanadium oxide.

For the samples with loading amounts of vanadium oxide below 3.2 mmol V/100 m^2 TS, increasing the loading amounts of copper oxide does not result in the appearance of new diffraction peaks, except the peak at 2θ = 38.8° is obviously intensified at 2.0 mmol Cu/100 m^2 TS, as shown in Figure 1a−c. Although the diffraction peaks of crystalline CuO cannot be distinguished quantitatively in these samples, the peak enhancement means that crystalline CuO is formed.

For 32 V/TS sample, dramatic changes take place. Sharp peaks, corresponding to characteristic diffractions of crystalline V_2O_5, appear at 2θ = 15.4, 20.3, 26.1, and 31.0°.[26] These peaks

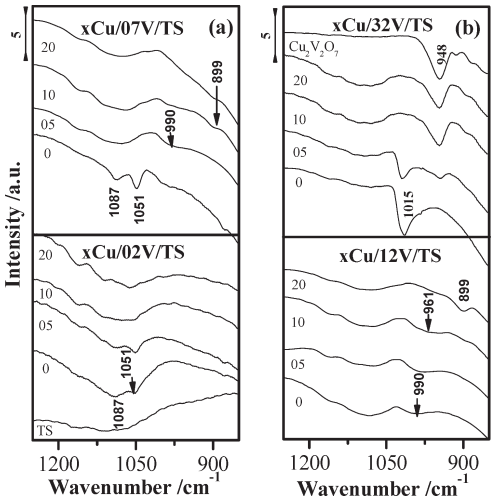

Figure 2. IR spectra of various *x* Cu/*y* V/TS samples.

lose intensity steadily following the copper oxide loadings and finally disappear at 20 Cu/32 V/TS sample. Simultaneously, two new peaks, which are corresponding to the characteristic diffractions of crystalline $Cu_2V_2O_7$ species, appear at 2θ = 24.7 and 28.9°. These phenomena reveal that copper oxide has strong interaction with vanadium oxide, resulting in the formation of $Cu_2V_2O_7$ species at certain loading amounts of both oxides, that is, 2.0 mmol Cu/100 m^2 TS and 3.2 mmol V/100 m^2 TS.

3.2. IR Results. IR spectra of *x* Cu/*y* V/TS samples ranging from 850 to 1250 cm^{-1} are shown in Figure 2. The spectra of 02 V/TS and 07 V/TS samples are predominated by two bands appearing at ∼1087 and ∼1051 cm^{-1}, respectively, as shown in Figure 2a. The ∼1087 cm^{-1} band is assigned to characteristic vibrations of TS mixed oxide, as observed in the TS sample. For the ∼1051 cm^{-1} band, previous studies confirmed that at a lower loading amount, vanadium oxide species are highly dispersed on the support, existing as isolated VO_x species and giving rise to a band at ∼1049 cm^{-1}.[27−29] Combined with the XRD results in Figure 1, it is reasonable to assign the ∼1051 cm^{-1} band to characteristic vibrations of dispersed vanadium oxide species on TS support. For *x* Cu/02 V/TS and *x* Cu/07 V/TS samples, the ∼1051 cm^{-1} band loses intensity gradually following the copper oxide loadings and disappears at certain copper oxide loadings. See the 10 Cu/02 V/TS and 05 Cu/07 V/TS samples, respectively.

Meanwhile, a new band corresponding to vibration of dispersed vanadium oxide species in two-dimension patches appears at 990 cm^{-1} for *x* Cu/07 V/TS samples.[26] The broad band at ∼990 cm^{-1} is also detected in the 12 V/TS sample, which generally intensifies and red shifts to ∼899 cm^{-1} with the loading amount of copper oxide increased to 2.0 mmol Cu/100 m^2 TS. Considering that the radius of Cu^{2+} (Paulling radius = 72 pm) is larger than that of V^{5+} (Paulling radius = 59 pm), it can be inferred that the Cu−O band length is larger than that of V−O, and this leads to a decrease in the force constant (k) of the band. The atomic weight of copper is also greater than that of vanadium, causing the increase of the reduced mass (μ). Hence, the vibration frequencies decrease according to the formula $\nu = (1/2\pi c)(k/\mu)^{1/2}$.[30] These spectral changes indicate that the presence of copper oxide alters the states of dispersed vanadium oxide, i.e., the interaction between copper oxide and preloaded vanadium oxide species takes place and V−O−Cu bands have been formed.

dx.doi.org/10.1021/cs200045f |ACS Catal. 2011, 1, 468–480

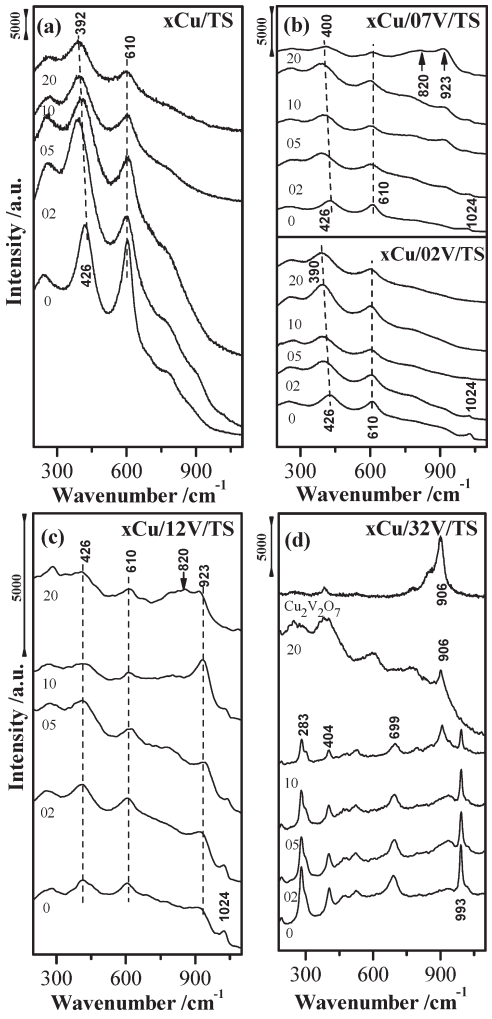

Figure 3. Raman spectra of various *x* Cu/*y* V/TS samples.

The spectra of *x* Cu/32 V/TS samples are obviously different from those with lower vanadium oxide loadings. There is a sharp band appearing at ~1015 cm^{-1} in 32 V/TS sample. This band corresponds to the characteristic stretching band of crystalline V_2O_5. The ~1015 cm^{-1} band loses intensity evidently following the copper oxide loadings, and disappears when the loading amount of copper oxide reaches 1.0 mmol Cu/100 m^2 TS. At 1.0 mmol Cu/100 m^2 TS and higher, a new band assigned to the characteristic vibration of $Cu_2V_2O_7$ species appears at 948 cm^{-1}. This band gains considerable intensity following the copper oxide loadings. These phenomena suggest that crystalline $Cu_2V_2O_7$ is the predominating species in *x* Cu/32 V/TS samples, with loading amounts of copper oxide ≥ 1.0 mmol Cu/100 m^2 TS. This is in agreement with the XRD results.

3.3. LRS Results. Figure 3 shows Raman spectra of *x* Cu/*y* V/TS samples ranging from 200 to 1100 cm^{-1}. For *x* Cu/TS samples, two strong bands assigned to characteristic vibrations of TS mixed oxide appear at ~426 and ~610 cm^{-1}, as shown in Figure 3a. The ~426 cm^{-1} band is red-shifted to 392 cm^{-1} when the loading amount of copper oxide is increased to 2.0 mmol Cu/100 m^2 TS. In contrast, the ~610 cm^{-1} band remains unchanged. These changes should be related to the interaction between copper oxide and TS support.[31]

For 02 V/TS and 07 V/TS samples, a new band appears at ~1024 cm^{-1}, which corresponds to the characteristic vibration of *V* = O in isolated VO_x species,[32] as shown in Figure 3b. The ~1024 cm^{-1} band disappears at certain loading amounts of copper oxide: 0.5 mmol Cu/100 m^2 TS for *x* Cu/02 V/TS catalysts and 2.0 mmol Cu/100 m^2 TS for the *x* Cu/07 V/TS sample. This suggests that an interaction between copper oxide and vanadium oxide occurs. A red shift of the ~426 cm^{-1} band following the copper oxide loadings is also observed, indicating that copper oxide also interacts with the TS support. Furthermore, compared with *x* Cu/02 V/TS samples, the spectra of *x* Cu/07 V/TS samples are changed significantly. Two bands at ~820 and ~923 cm^{-1} can be clearly observed when the loading amounts of copper oxide are higher than 0.5 mmol Cu/100 m^2 TS. Both bands correspond to the vibrations of V−O−V bonds in two-dimension vanadium oxide patches.[32]

For the 12 V/TS sample, the three bands at ~426, ~610, and ~1024 cm^{-1} can also be observed. The appearance of the ~923 cm^{-1} band means that V−O−V bonds have been formed at this loading amount of vanadium oxide. This band gains intensity significantly following the copper oxide loadings, as shown in *x* Cu/12 V/TS samples in Figure 3c. On the other hand, the ~1024 cm^{-1} band is weakened and is not detectable in 20 Cu/12 V/TS sample. Moreover, the band at ~426 cm^{-1} remains unchanged with the increase in copper oxide loadings. These results indicate that when the copper oxide species are introduced into the samples, the amount of isolated VO_x species reduces gradually, and they transform into polymeric VO_x species due to the strong interaction between copper oxide and vanadium oxide species and the formation of V−O−Cu species. In contrast, the interaction between copper oxide species and TS support has been weakened.

The Raman spectrum for 32 V/TS sample is quite different from those with lower loading amounts of vanadium oxide. There are four predominant bands appearing at ~283, ~404, ~699, and ~993 cm^{-1}, which correspond to the characteristic vibrations of crystalline V_2O_5, as shown in Figure 3d.[32,33] Combined with XRD results, this result proves that at this loading amount of vanadium oxide, crystalline V_2O_5 is the primary species on the surface of TS support. These bands lose intensities proportionately following the copper oxide loadings. The band associated with crystalline $Cu_2V_2O_7$ at ~906 cm^{-1} appears in 10 Cu/32 V/TS and 20 Cu/32 V/TS samples, indicating that crystalline $Cu_2V_2O_7$ has been formed at these high copper oxide loadings. These are in agreement with XRD and IR results.

Following above IR and Raman results, we describe the copper oxide−vanadium oxide interaction in Cu/V/TS samples in which there is no V_2O_5 and $Cu_2V_2O_7$ formation. The interaction is schematically shown in Figure 4. When copper oxide is absent (i.e., *y* V/TS samples), the isolated VO_x species (Figure 4b) predominate on the surface of the TS support (Figure 4a) at low loading amounts of vanadium oxide (≤0.7 mmol V/100 m^2 TS) in this study. Polymeric VO_x species (Figure 4c) appear and transform into crystalline vanadia at higher loading amounts (e.g., 3.2 mmol V/100 m^2 TS). When copper oxide is postloaded, the strong interaction between copper oxide and vanadium oxide induces the isolated VO_x species to transform into the polymeric VO_x species, and V−O−Cu bands are also formed (Figure 4d). In addition, for *x* Cu/12 V/TS samples, the strong copper oxide−vanadium oxide interaction renders the interaction between copper oxide and TS support obviously weak. This should

dx.doi.org/10.1021/cs200045f |*ACS Catal.* 2011, 1, 468–480

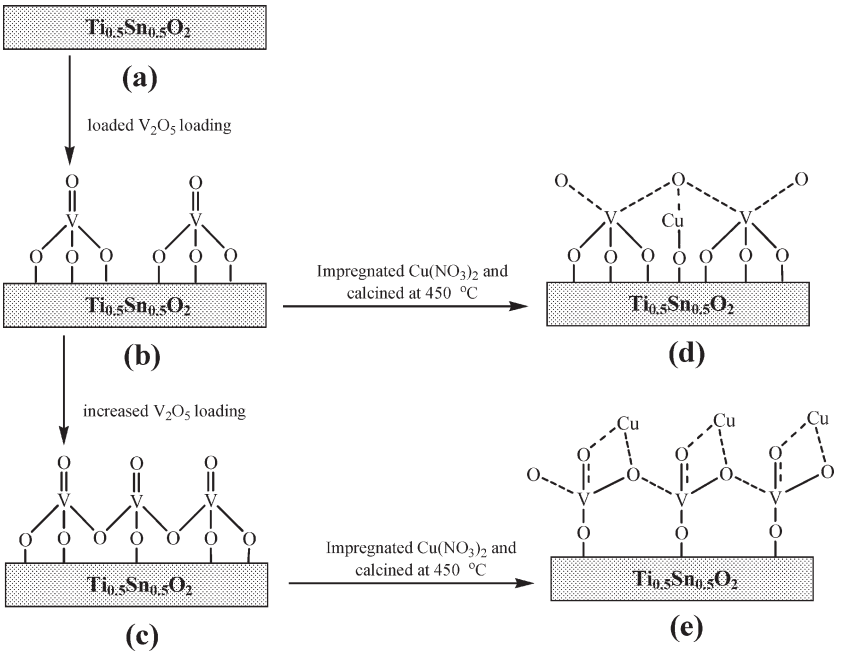

Figure 4. Schematic diagram of the interaction mode between copper oxide and surface dispersed vanadium oxide.

be attributed to the hindrance of the dominant polymeric vanadium oxide species on the surface of TS support (Figure 4e).

3.4. TPR Results. H_2 consumption in the TPR profile of TS sample (see Figure 5a) becomes appreciable above 200 °C. Only one broad peak (~300 °C) can be observed in the profile, which should be attributed to the reduction of Ti^{4+} (Sn^{4+}) ions on the surface of the TS support. The TPR profiles of *y* V/TS samples cover the same temperature scale as that for TS, but the single peak gains a much stronger intensity, with a maximum at ~300 °C, as shown in the bottom profiles of Figure 5b−e. For *x* Cu/TS samples (Figure 5a), the TPR profiles are complicated: H_2 consumption is extended to a lower temperature region following the copper oxide loadings; meanwhile, the lower H_2 consumption gains intensities dramatically with the increase in the copper oxide loadings. Evidently, the lower temperature H_2 consumption is associated with the reduction of copper oxide.

To get insight into the surface copper oxide species, we did curve fitting by Gaussian curves for all the profiles. See the dot lines in each profile. It can be seen that there is more than one type of copper oxide existing in *x* Cu/TS samples, and reduction of these copper oxide species is mainly below 250 °C. According to the literature,[34,35] the sharp peak at ~150 °C is associated with reduction of surface dispersed copper oxide that weakly interacts with the TS support. The peaks appearing between 200 and 250 °C are associated with reduction of the surface dispersed copper oxide species that strongly interacts with the TS support (see the 05 Cu/TS profile).

For *x* Cu/02 V/TS samples, the TPR profiles resemble those of *x* Cu/TS samples, except that all the peaks assigned to the reduction of copper oxide species (below 250 °C) shift to a higher temperature region. The profiles of *x* Cu/07 V/TS and *x* Cu/12 V/TS samples are very different from those of *x* Cu/02 V/TS samples. Throughout the copper oxide loadings, two peaks are detected, as shown in Figure 5c and d. By comparison, it can be seen that (1) irrespective of vanadium oxide loading, increasing copper oxide loading always results in the predominant peak (the lower temperature one) shifting to lower temperature; (2) irrespective of copper oxide loading, increasing vanadium oxide loading always induces the low temperature peaks to shift to higher temperatures (compare the profiles following a same loading amount of copper oxide but different loading amounts of vanadium oxide); (3) the second peak (the higher temperature one), which possesses very low intensities at a low loading amount of copper oxide (i.e., 0.5 and 1.0 mmol Cu/100 m^2 TS), gains considerable intensities in the profiles of 20 Cu/*y* V/TS samples. Overall, by comparing with the profiles of *x* Cu/TS (Figure 5a) and *y* V/TS samples, it is reasonable to assign these peaks as follows: the low temperature peaks (the predominant one in each profile) are probably associated with the reduction of dispersed CuO and V−O−Cu species, and the high temperature peaks are mainly assigned to the reduction of vanadium oxide species. It is worth mentioning that at higher loading amounts of copper oxide (i.e., 2.0 mmol Cu/100 m^2 TS), since XRD results (Figure 1) have proved crystalline CuO is formed, the high temperature peaks can also be associated with a reduction of crystalline CuO. Moreover, these results also confirm that the presence of copper oxide promotes the reduction of vanadium oxide, but the presence of vanadium oxide suppresses the reduction of copper oxide.

H_2 consumption in *x* Cu/32 V/TS profiles gives rise to a very broad peak ranging from 200 to 400 °C, in which temperature scale several peaks can be distinguished. The lowest temperature peak in each profile can be assigned to the reduction of V−O−Cu species, the other peaks at higher temperatures can be assigned to reduction of V_2O_5 and $Cu_2V_2O_7$ species, because the above XRD, IR, and LRS results have confirmed that crystalline V_2O_5 and $Cu_2V_2O_7$ have been formed at this loading amount of vanadium oxide. In addition, for all *x* Cu/*y* V/TS samples, H_2 consumption can be observed above 400 °C, corresponding to the reduction of bulk TS, moreover, H_2 consumption gains intensities dramatically at the higher temperature (~650 °C), for simplicity, this temperature region (above 400 °C) is not shown in the profiles. It is noteworthy that, for 10 Cu/TS and 20 Cu/TS

dx.doi.org/10.1021/cs200045f |*ACS Catal.* 2011, 1, 468–480

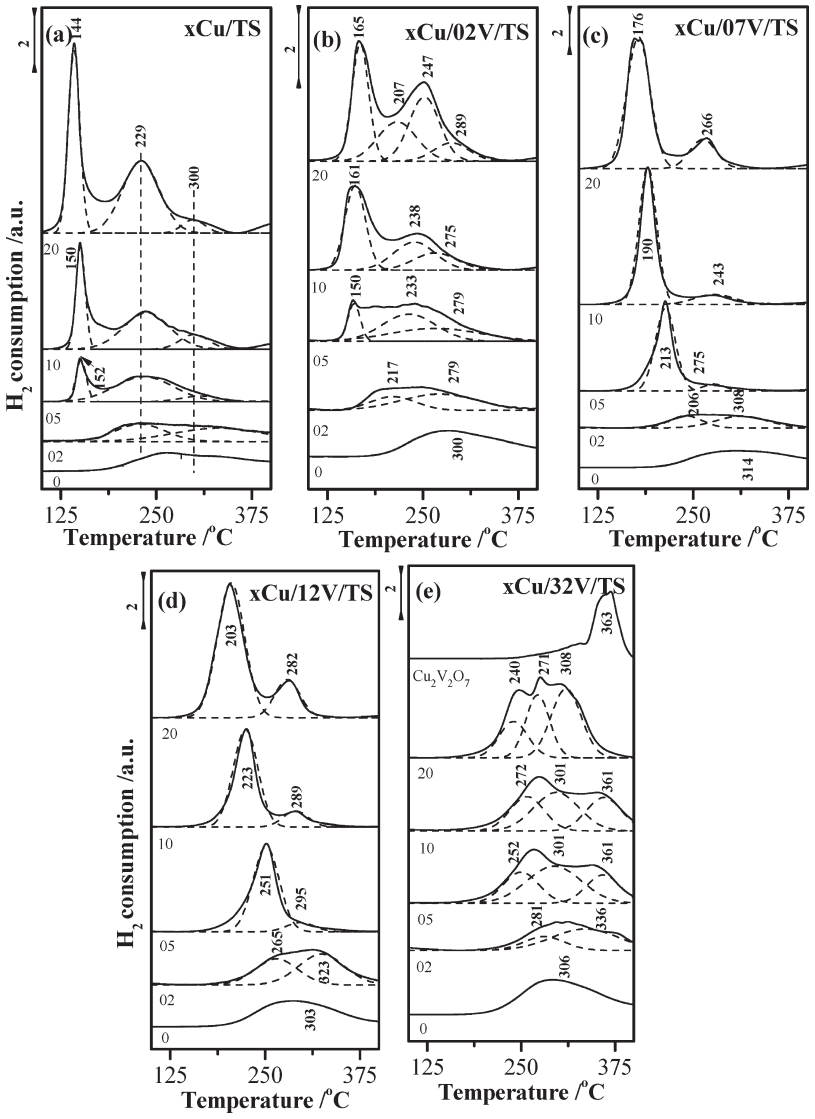

Figure 5. TPR profiles of (a) *x* Cu/TS; (b) *x* Cu/02 V/TS; (c) *x* Cu/07 V/TS; (d) *x* Cu/12 V/TS, and (e) *x* Cu/32 V/TS samples (*x* = 0, 02, 05, 10, 20).

Table 1. TPR Fitting Results of 10 Cu/*y* V/TS Samples with Different Vanadium Oxide Loadings

	temperature (°C)		intensity (a.u.)		
sample	peak I	peak II	peak I	peak II	peak I/II ratio
10 Cu/TS	150, 229	300	120.1	27.6	4.35
10 Cu/02 V/TS	161, 238	275	125.3	25.4	4.93
10 Cu/07 V/TS	190	243	165.6	25.5	6.49
10 Cu/12 V/TS	223	289	160.4	30.3	5.29

samples, H_2 consumption can be observed from 360 °C due to the interaction between more copper oxides and TS support.

We further investigate how the reduction of *x* Cu/*y* V/TS samples depends on the loading amount of vanadium oxide (loading amount of copper is fixed), and take 10 Cu/*y* V/TS samples as an example. The peak position (indicated as temperature), peak intensities and peak intensity ratios are shown in Table 1. With the increase in vanadium oxide loadings, the low temperature reduction peaks below 250 °C (designated I) are shifted to high temperature, and the intensities increase gradually. In contrast, the high temperature reduction peaks beyond 250 °C (designated II) are shifted to low temperature, and the intensities remain almost constant. According to the above discussions, it can be concluded that the strong interaction between the dispersed vanadium oxide and copper oxide species on the surface of TS support (i.e., formation of V−O−Cu species) makes it more difficult to reduce copper oxide species. Furthermore, it is noteworthy that for 10 Cu/*y* V/TS samples, both the intensity of the low temperature peak and the intensity ratio of the low temperature peak to the high temperature peak reach a maximum at the 10 Cu/07 V/TS sample, suggesting that much more V−O−Cu species should be formed in the 10 Cu/07 V/TS sample.

On the basis of these results, it can be concluded that a strong interaction exists between copper oxide and vanadium oxide. Due to this strong interaction, V−O−Cu species are formed and the reduction of dispersed copper oxide becomes more difficult, but the reduction of vanadium oxide is easier.

dx.doi.org/10.1021/cs200045f |*ACS Catal.* 2011, 1, 468–480

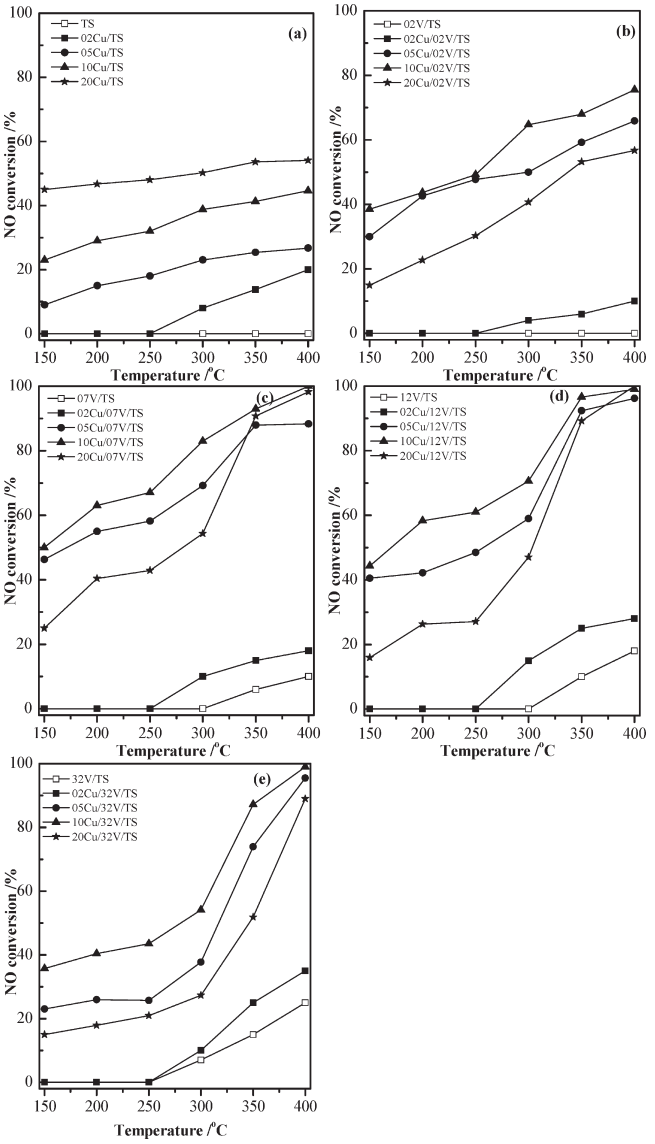

Figure 6. NO conversion on (a) *x* Cu/TS, (b) *x* Cu/02 V/TS, (c) *x* Cu/07 V/TS, (d) *x* Cu/12 V/TS, and (e) *x* Cu/32 V/TS catalysts (*x* = 0, 02, 05, 10, 20).

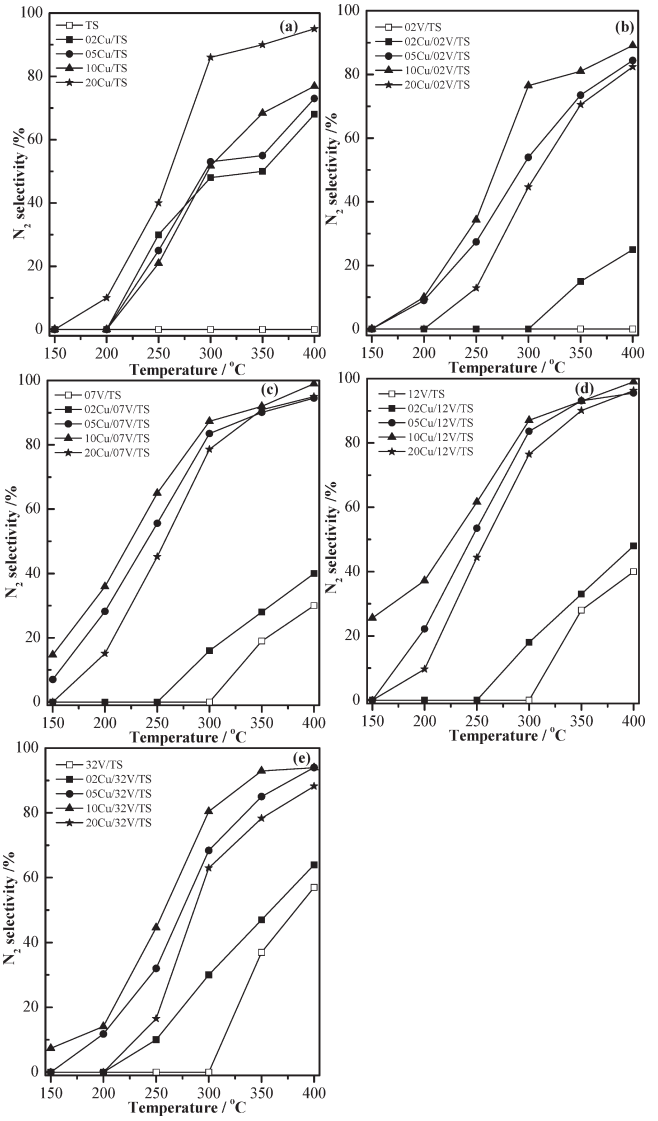

Figure 7. N_2 selectivity on (a) *x* Cu/TS, (b) *x* Cu/02 V/TS, (c) *x* Cu/07 V/TS, (d) *x* Cu/12 V/TS, and (e) *x* Cu/32 V/TS catalysts (*x* = 0, 02, 05, 10, 20).

3.5. Activities of *x* Cu/*y* V/TS Catalysts in NO + CO Reaction. The activities of *x* Cu/*y* V/TS catalysts in the NO + CO reaction, which are shown in terms of NO conversion and N_2 selectivity, are presented in Figures 6 and 7, respectively. Several interesting features can be deduced from the figures:

(1) For *x* Cu/TS catalysts (Figure 6a), NO conversions increase proportionately following the copper oxide loadings and reach a maximum over 20 Cu/TS catalyst. Increasing the operating temperature slightly promotes NO conversions.

(2) NO conversions of *y* V/TS catalysts are not detectable at the operating temperatures between 25 and 300 °C, but reach ~20% at 350 and 400 °C when the loading amounts of vanadium oxide are ≥0.7 mmol V/100 m^2 TS (see the bottom curve in Figure 6b−e). Therefore, it can be suggested that the vanadium oxide species in the catalysts have limited reactivity to NO + CO reaction.

(3) Compared with *x* Cu/TS and *y* V/TS catalysts, NO conversion over *x* Cu/*y* V/TS catalysts is significantly enhanced. The higher activity may be associated with the interaction between copper oxide and vanadium oxide, i.e., the formation of V−O−Cu species. As displayed in Figure 6b−e, when the loading amount of copper oxide is increased, NO conversion increases initially and decreases over 20 Cu/*y* V/TS catalysts, indicating that increasing the copper oxide loading cannot always promote the catalytic activity. Among *x* Cu/*y* V/TS catalysts, maximum NO conversions are always achieved on 10 Cu/*y* V/TS catalysts. In addition, variations in selectivity to N_2 are consistent with that of the NO conversion for all catalysts. Moreover, during low temperature reaction, N_2O as the main reaction product can be detected. The results suggest that the formation of larger CuO particles does not contribute to the catalytic activity. On the other hand, the decrease in the activity may also be due to the formation of crystalline CuO, which covers V−O−Cu

dx.doi.org/10.1021/cs200045f |*ACS Catal.* 2011, 1, 468–480

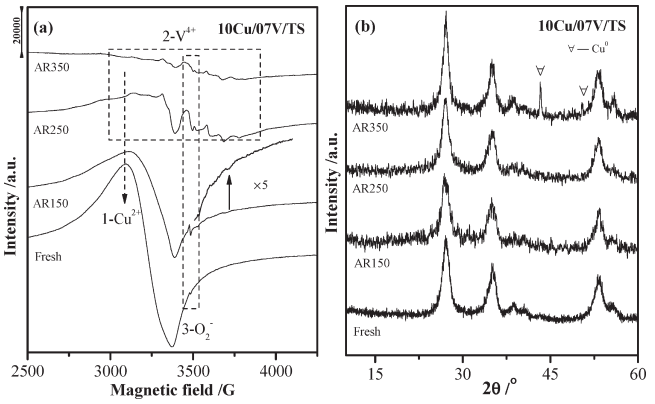

Figure 8. EPR spectra (a) and XRD patterns (b) of fresh and after reaction of a 10 Cu/07 V/TS sample at various temperatures (AR150, AR250, and AR350).

species. Compared with the activities of 10 Cu/*y* V/TS catalysts, it can be seen that NO conversion reaches a maximum at 10 Cu/07 V/TS catalyst under the same temperature scale; for example, NO conversions at 150, 250, and 350 °C are 50.7%, 67.1%, and 93.2%, respectively. For 10 Cu/12 V/TS catalyst, the decrease in the NO conversion can be attributed to the hindrance of the polymeric vanadium oxide species, which results in the copper oxide's dispersing on the surface of the vanadium oxide (Figure 4e), so the V−O−Cu species dispersed on the TS support decrease. Further increasing the vanadium oxide loadings (i.e., 10 Cu/32 V/TS catalyst), the crystalline $Cu_2V_2O_7$ forms on the surface of the catalyst, which leads to the further decrease in NO conversion. Combined with the results discussed above, it seems reasonable to conclude that the dispersed V−O−Cu species contribute to the high catalytic activity of NO + CO reaction.

These features convey insightful information on the performances of *x* Cu/*y* V/TS catalysts in NO + CO reaction. The dispersed V−O−Cu species are the main active component for *x* Cu/*y* V/TS catalysts. The contribution of the vanadium oxide species, crystalline CuO, and $Cu_2V_2O_7$ to the reaction is limited.

3.6. EPR and XRD Results. To further explore the active species of *x* Cu/*y* V/TS samples toward NO + CO reaction, EPR characterization was conducted for the 10 Cu/07 V/TS sample. Note that this sample indicates a best performance in the reaction. Figure 8a shows the EPR spectra of the 10 Cu/07 V/TS sample before and after reaction at various temperatures. For a fresh 10 Cu/07 V/TS sample, a strong axially symmetric signal (designated 1) associated with Cu^{2+} ions is observed,[34,35] and no signal for vanadium oxide species is present. After reaction at 150 °C (denoted as AR150) and 250 °C (denoted as AR250), the intensities of Cu^{2+} species obviously decrease, but a set of hyperfine lines for V^{4+} species (designated 2) appear and are intensified after reaction at 150 °C. These are ascribed to the interaction of the unpaired electron with the ^{51}V nucleus ($I = 7/2$) subjected to an axial crystal field.[36] However, after the sample was put into the reaction at 350 °C (denoted as AR350), Cu^{2+} signals almost disappear, and the intensities of V^{4+} signals also decrease. In the meantime, a sharp signal (designated 3) appears, which is ascribed to paramagnetic O_2^- species resulting from the oxygen vacancy.[37] For AR250 and AR350 samples, the signal is not distinguishable due to its overlapping with V^{4+} signals. The spin Hamiltonian parameters are reported in Table 2.

Table 2. EPR Spin Hamiltonian Parameters of Fresh and after Reaction of 10 Cu/07 V/TS Sample at Various Temperatures (AR150, AR250 and AR350)

sample	signal	$g_\parallel$	$g_\perp$	$A_\parallel$ (G)	$A_\perp$ (G)	species
fresh	1	2.15	2.072	128	not resolved	Cu^{2+}
AR150	1	2.36	2.077	125	not resolved	Cu^{2+}
	2	1.92	2.011	186	77.7	V^{4+}
AR250	1	2.41	2.080	106	not resolved	Cu^{2+}
	2	1.92	2.010	187	77.8	V^{4+}
AR350	2	1.94	2.030	184	79.7	V^{4+}
all	3	2.00	1.990			O_2^-

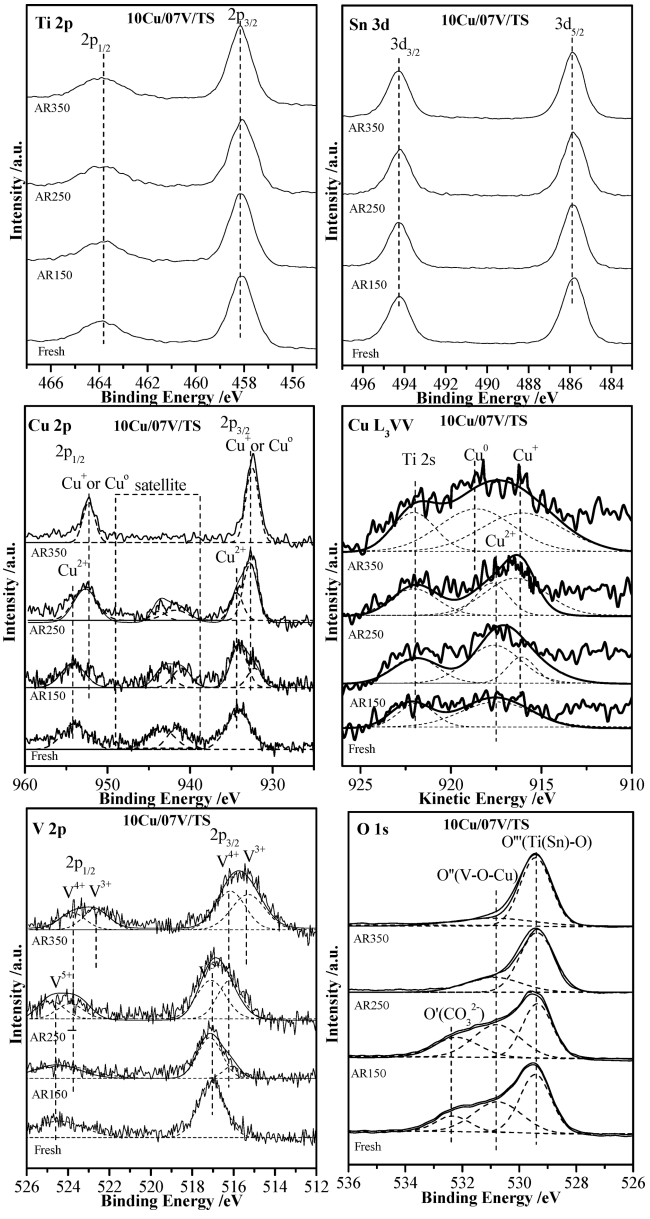

Figure 9. XP spectra of fresh and after reaction of a 10 Cu/07 V/TS sample at various temperatures (AR150, AR250 and AR350).

dx.doi.org/10.1021/cs200045f |ACS Catal. 2011, 1, 468–480

Table 3. Peak Positions (in eV) Relative to C 1s (285.0 eV) and Atomic Concentration % for the Core Levels Cu $2p_{3/2}$, Cu L_3VV, V $2p_{3/2}$, O 1s, Ti $2p_{3/2}$, and Sn $3d_{5/2}$

	Cu $2p_{3/2}$			Cu L_3VV/atomic concentration%			V $2p_{3/2}$/atomic concentration%			O 1s				
sample	Cu^{2+}	Cu^+ or Cu^0	Cu_{sat}/Cu_{main}[a]	Cu^{2+}	Cu^+	Cu^0	V^{5+}	V^{4+}	V^{3+}	O′	O″	O‴	Ti $2p_{3/2}$	Sn $3d_{5/2}$
fresh	934.1		0.85	917.5/100			517.1/100			532.3	530.7	529.4	458.1	485.8
AR150	934.1	932.2	0.76	917.5/69.7	916.2/30.3		517.1/79.6	516/20.4		532.3	530.7	529.4	458.1	485.8
AR250	934.1	932.2	0.23	917.5/32.6	916.2/67.4		517.0/52.5	516.1/47.5			530.7	529.4	458.1	485.8
AR350		932.3	0		916.2/54.4	918.6/45.6		516.1/45.4	515.3/54.6		530.7	529.4	458.1	485.8

[a] Cu_{main}, Cu $2p_{3/2}$ main line; Cu_{sat}, Cu $2p_{3/2}$ satellite.

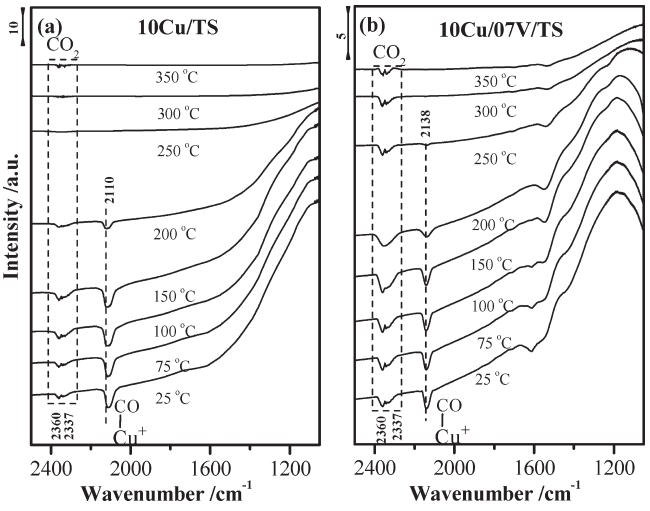

Figure 10. In situ FT-IR spectra of CO interaction with (a) 10 Cu/TS and (b) 10 Cu/07 V/TS samples from 25 to 350 °C.

It can be seen that the $g_{\|}$ values corresponding to Cu^{2+} and V^{4+} signals shift from 2.15 to 2.41 and from 1.92 to 1.94, respectively. Since previous studies have proved that environment of a paramagnetic ion can be obtained directly by comparing its spin Hamiltonian parameters, these results suggest that the coordinative environment of copper and vanadium species are changed in the process of reaction.

To experimentally confirm the valence changes of copper species with an increase in the operating temperatures under NO + CO atmosphere, the XRD patterns of the 10 Cu/07 V/TS sample before and after reaction at various temperatures were recorded, as shown in Figure 8b. It can be seen that the characteristic peaks of metallic Cu^0 (2θ = 43.2 and 50.3°) appear when the operating temperature is increased to 350 °C, indicating copper oxides reduced into Cu^0 species.

3.7. XPS Results. To further explore the valence changes of copper and vanadium species during NO + CO reaction, XPS measurements were carried out over a 10 Cu/07 V/TS sample before and after the NO + CO reaction at different temperatures, as shown in Figure 9, and the peaks were fitted by Gaussian curves. The binding energies, $Cu_{sat.}/Cu_{main}$, and atomic concentration are listed in Table 3. For all samples, the binding energies of Ti^{4+} and Sn^{4+} are located at 458.1 (Ti $2p_{3/2}$) and 485.8 eV (Sn $3d_{5/2}$), respectively.[38,39] The position is not obviously changed under NO + CO atmosphere at different temperatures, implying that the TS support is stable in the reaction course.

For the fresh sample, only the characteristic peak assigned to Cu^{2+} (Cu $2p_{3/2}$) ions appears at 934.1 eV, with a satellite peak at 940.6−943.4 eV.[40−42] For after-reaction samples, with the increase in reaction temperature, the peak is weakened gradually and disappears completely at 350 °C. Meanwhile, the lower Cu $2p_{3/2}$ binding energies at 932.2 eV corresponding to the lower valence copper species is present. In addition, it can be seen that the relative intensities of the satellite peak with respect to the main peak gradually decrease from 0.85 to 0, as shown in Table 3, which further confirms the appearance of the low valence copper species. However, the Cu 2p binding energies cannot be used to distinguish between Cu^+ and Cu^0 because they are essentially identical. Thus, the Cu L_3VV Auger spectra (Figure 9) were performed to distinguish the variety of the copper species (Cu^{2+}, 917.5 eV; Cu^+, 918.6 eV; Cu^0, 916.2 eV).[42] The concentrations of Cu^0, Cu^{2+}, and Cu^+ are listed in Table 3. As can be seen, for fresh and AR150 samples, Cu^{2+} is the main copper species, whereas Cu^{2+} (69.3%) and Cu^+ (30.7%) are present in the AR250 sample, and Cu^+ (54.4%) and Cu^0 (45.6%) coexist in AR350 sample.

Concerning the valence changes of V species, it is clear that in fresh and AR150 samples, only V^{5+} (517.1 eV) is mainly present. However, V^{4+} (516.1 eV) and V^{3+} (515.3 eV) can be observed in AR250 and AR350 samples, respectively.[43,44] Moreover, the concentrations of V^{5+} and V^{4+} are 62.5% and 37.5% in the AR250 sample, respectively, as well as V^{4+} (45.4%) and V^{3+} (54.6%) are present in the AR350 sample, as shown in Table 3.

In Figure 9, O 1s spectra show three peaks centered at 532.3 (O′), 530.7 (O″), and 529.4 eV (O‴). According to the literature,[38,45,46] the O′ and O‴ are attributed to the oxygen of CO_3^{2-} and lattice oxygen associated with TS, respectively. The lattice oxygen of TS is almost unchanged in the whole reaction temperature region, and the oxygen of CO_3^{2-} disappears at 250 °C due to its low stability. Moreover, it is noteworthy that the changes of the O″ species are different from the others. The intensity of the peak O″ significantly decreases at 250 °C and almost disappears at 350 °C. According to the above Cu 2p and V 2p results (which have confirmed that Cu^{2+} and V^{5+} have been simultaneously reduced to the lower valence), it seems reasonable to assign O″ ions to the oxygen of V−O−Cu species, and the reduction of V−O−Cu species results in O″ species' disappearing.

Following the above results, it can be concluded that when the temperature is below 250 °C, Cu^{2+} and V^{5+} of V−O−Cu species are reduced to Cu^+ and V^{4+} under a reaction atmosphere, respectively. When the temperature is higher than 250 °C, the reductions of Cu^+ to Cu^0 and V^{4+} to V^{3+} take place simultaneously.

As reported previously,[47−49] vanadium species are active to decompose NO in V−O−W/Ti(Sn)O_2 and V−O−Mo/Ti(Sn)O_2 systems, and Cu^{2+}/Cu^+ or Cu^+/Cu^0 redox couples are effective for selective catalytic reduction of NO by CO. Combined with the above results, it is reasonable to follow that

dx.doi.org/10.1021/cs200045f |ACS Catal. 2011, 1, 468–480

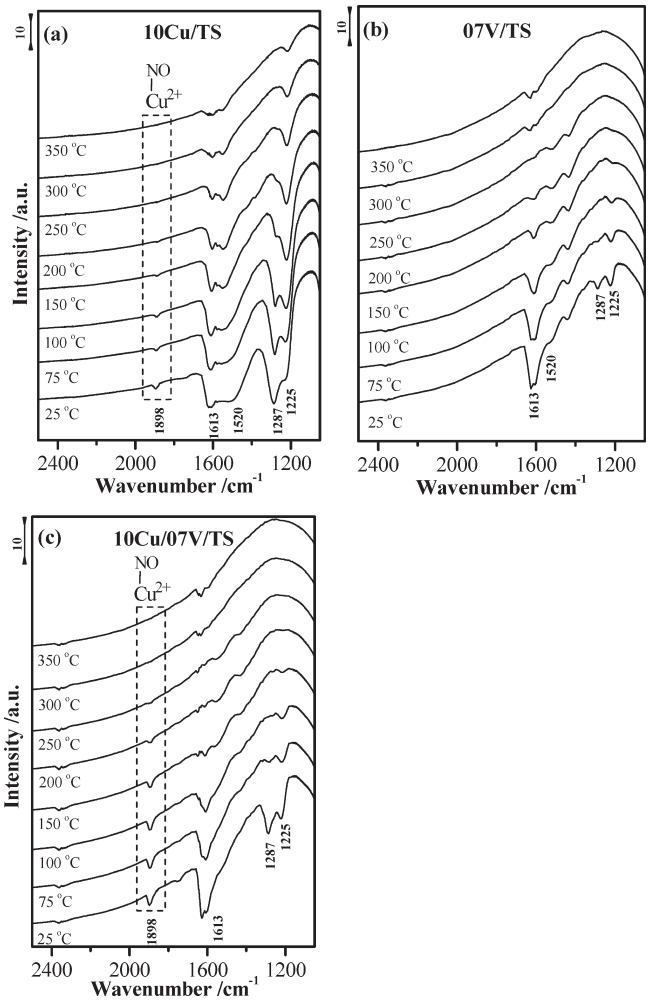

Figure 11. In situ FT-IR spectra of NO interaction with (a) 10 Cu/TS, (b) 07 V/TS, and (c) 10 Cu/07 V/TS samples from 25 to 350 °C.

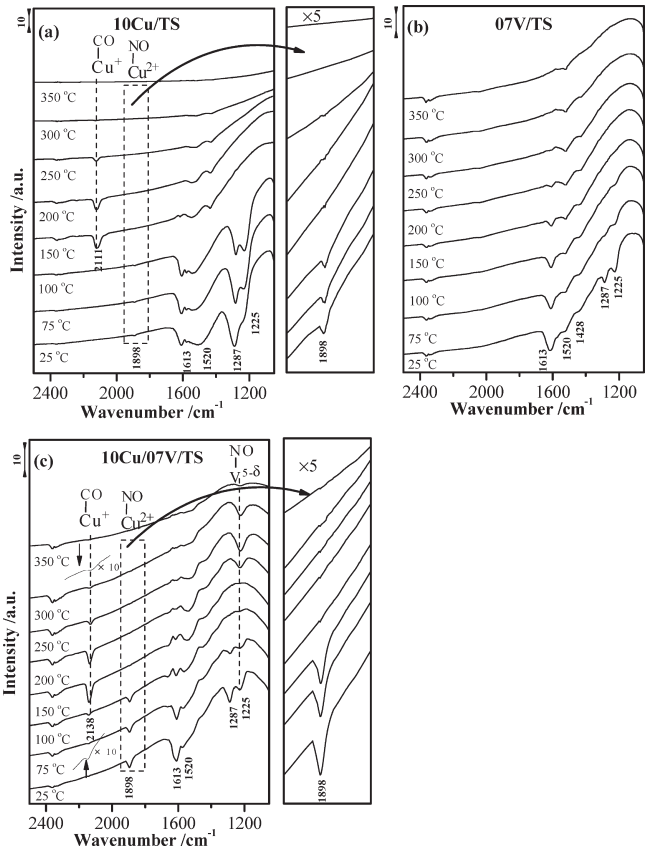

Figure 12. In situ FT-IR spectra of CO and NO co-interaction with (a) 10 Cu/TS; (b) 07 V/TS, and (c) 10 Cu/07 V/TS samples from 25 to 350 °C.

the NO + CO reaction over Cu/V/TS samples may proceed through different mechanisms at low and high temperatures, being a result of the change of active species. Cu^{2+}/Cu^{+} and V^{5+}/V^{4+} couples play an important role below 250 °C, whereas the reductions of Cu^{+}/Cu^{0} and V^{4+}/V^{3+} groups make great contributions to NO reduction at higher than 250 °C.

3.8. IR Spectra of CO Adsorbed on *x* Cu/*y* V/TS Samples. Exposure of a 07 V/TS sample to a CO stream in the temperature regions between 25 and 350 °C does not give rise to any characteristic bands related to CO vibrations; that is, no CO molecules are adsorbed on such a sample at current operating conditions. Hence, for brevity, the spectra are not shown. For the 10 Cu/TS sample (Figure 10a), the characteristic band associated with adsorbed CO molecules appears at ~2110 cm^{-1} at 25 °C, remains constant below 100 °C, but decreases greatly at 200 °C and disappears when the temperature increases to 250 °C. Considering our previous investigation,[17,18] this band should be due to the CO molecules adsorbed on Cu^{+} sites to form the linear CO−Cu^{+} species. The reduction of Cu^{+} ions to Cu^{0} results in the disappearance of adsorption on Cu^{+}.

The adsorption of CO species is also observed in the 10 Cu/07 V/TS sample at 25 °C and higher temperature; however, the band is evidently blue-shifted to ~2138 cm^{-1}, as shown in Figure 10b. A similar phenomenon was observed in our previous $CuO/WO_3/Ce_xZr_{1-x}O_2$ system,[50] which is ascribed to the interaction between copper oxide and tungsten oxide. This corroborates the previous conclusion that the strong interaction occurs between the copper oxide and vanadium oxide and that V−O−Cu species have been formed. Moreover, since the vibrational frequency does not change greatly with the temperature from 25 to 250 °C (the band disappears at 300 °C), it can be suggested that the states of copper oxide species do not undergo significant changes, and the copper oxide species are more difficult to reduce than those in 10 Cu/TS sample. This is consistent with the TPR result. It is worth mentioning that there are two peaks at 2337 and 2360 cm^{-1} for these two samples, which is attributed to the characteristic vibration of CO_2. This further confirms that the surface copper oxide is reduced by CO.

3.9. IR Spectra of NO Adsorbed on *x* Cu/*y* V/TS Samples. IR spectra of NO adsorption on *x* Cu/*y* V/TS samples are much more complicated than those of CO adsorption. For the 10 Cu/TS sample, several bands appear at 25 °C, assigned to the characteristic vibration of the Cu^{2+}−NO (ν(N═O)) species (~1898 cm^{-1}) and NO_3^- species; that is, the ν(N═O) of bridged bidentate NO_3^- (~1520 cm^{-1}) and chelated bidentate NO_3^- (~1613 cm^{-1}) and the $\nu_{as}(NO_2)$ of bridged bidentate NO_3^- (~1225 cm^{-1}) and chelated bidentate NO_3^- (~1287 cm^{-1}), respectively,[51−53] as shown in Figure 11a. All the bands decrease with increasing temperature. Bands at both ~1898 and ~1287 cm^{-1} disappear at 250 °C; the other three bands still retain considerable intensities at 350 °C. For the 07 V/TS sample, the band at ~1613 cm^{-1} gains a much stronger

dx.doi.org/10.1021/cs200045f |ACS Catal. 2011, 1, 468–480

intensity at 25 °C than that in the 10 Cu/TS sample, as shown in Figure 11b. However, the bands at ~1225 and ~1287 cm^{-1} are much weaker, and the ~1898 cm^{-1} band is not detected. When the adsorption temperature increases, the ~1613 cm^{-1} band decreases; the ~1287 cm^{-1} band disappears at 75 °C, and the ~1225 cm^{-1} band disappears at 200 °C. These results suggest that NO is only weakly adsorbed on the 07 V/TS surface due to its lower surface basicity.[53]

The 10 Cu/07 V/TS sample resembles that of the 10 Cu/TS sample at 25 °C, with the exception that the ~1898 cm^{-1} band is much stronger and the ~1520 cm^{-1} band is not observable (Figure 11c). However, the spectra at the adsorption temperatures higher than 200 °C are similar to those following an exposure of the 07 V/TS sample to a NO stream in the same adsorption temperature scale. These results suggest that some copper oxide species still retain the same states as those in the 10 Cu/TS sample when the adsorption temperatures are below 250 °C. but the NO adsorption species with the temperature above 250 °C should be related to the vanadium oxide species in the 10 Cu/07 V/TS sample.

3.10. IR Spectra of NO + CO Adsorbed on *x* Cu/*y* V/TS Samples. IR spectra following the exposures of 10 Cu/TS, 07 V/TS, and 10 Cu/07 V/TS samples to a stream of NO + CO mixture are compared in Figure 12. For 10 Cu/TS sample (Figure 12a), the bands associated with vibration of Cu^{2+}−NO (ν(N═O)) species (~1898 cm^{-1}) are weakened gradually and disappear entirely at 150 °C. In addition, the band associated with CO molecules adsorbed on Cu^{+} sites (~2110 cm^{-1}) appears only at the adsorption temperatures between 150 and 250 °C. At higher adsorption temperatures (>100 °C), the NO_3^- bands diminish significantly and finally vanish. This is significant because it clearly indicates that NO_3^- bands persist to 350 °C following an exposure of 10 Cu/TS sample to a NO stream, as shown in Figure 11a. As such, it is reasonable to conclude that the NO_3^- species should be adsorbed on Cu^{2+} sites of the 10 Cu/TS sample, but Cu^{2+} species are unstable and easily reduced to Cu^{+} species in the NO + CO mixture. As a result, the characteristic bands of the NO_3^- species are not observable above 150 °C.

Simultaneously, CO adsorption species are observed on the reduced Cu^{+} species. Furthermore, these adsorption species are intimately related to the catalytic activity. Under the NO + CO mixture, the 10 Cu/TS sample can provide Cu^{+} and Cu^{2+} species, which can adsorb the CO molecules and NO molecules, respectively, at the low temperature (≤250 °C). Such adsorbed NO and CO molecules are the main species that take part in the reaction. Whereas, at the high temperature (>250 °C), the catalytic activity of 10 Cu/TS sample is almost unchanged or slightly increases. This should be related to the further reduction of Cu^{+} species to Cu^{0}, which cannot adsorb the CO molecules and NO species at that temperature region. For the 07 V/TS sample, the spectra are fairly consistent with those following an exposure of the 07 V/TS sample to a NO stream throughout the adsorption temperatures. In other words, the adsorption of NO on such a sample is not influenced by CO molecules, corroborating the conclusion that no CO molecules are adsorbed on the 07 V/TS sample.

Noticeably, for the 10 Cu/07 V/TS sample, the spectra present some striking features: (1) The band of CO at ~2138 cm^{-1} presents at 25 °C and gains significant intensity with an increase in the adsorption temperature to 150 °C, then decreases with further increase of the temperature and still remains at 350 °C. In contrast, the band of NO at ~1898 cm^{-1} gains intensity at 25 °C and gradually decreases with an increase in the temperature and then disappears at 150 °C. These results indicate that CO adsorption on the 10 Cu/07 V/TS sample is much more stable than on the 10 Cu/TS sample; that is, Cu^{+} is much more stable in the 10 Cu/07 V/TS sample than that in 10 Cu/TS sample. This is consistent with the above TPR and CO adsorption results. (2) The NO_3^- bands (1287 and 1225 cm^{-1}) become weak gradually and disappear entirely at 150 °C. This is consistent with that for the 10 Cu/TS sample and possibly accounts for the reaction activity for the 10 Cu/07 V/TS sample being similar to that of the 10 Cu/TS sample at the low temperature. (3) The ~1225 cm^{-1} band gains significant intensities at the adsorption temperatures between 250 and 350 °C, but this is not observed in the 10 Cu/TS sample. This can be reasonably related to the NO adsorbed on reduced vanadium species.[54] Taking into consideration the spectra following the exposures of the 10 Cu/TS sample to NO and the NO + CO mixture and the 10 Cu/07 V/TS sample to NO, we suggest that under the NO + CO mixture, the 10 Cu/07 V/TS sample can provide Cu^{+} and Cu^{2+} species that can adsorb the CO and NO molecules, respectively, at the low temperature (≤250 °C). Such adsorbed NO and CO molecules are the main species that take part in the reaction. Whereas, at the high temperature (>250 °C), the 10 Cu/07 V/TS sample provides Cu^{+} and reduced vanadium species, which can adsorb the CO molecules and NO species, respectively. These results further corroborate EPR and XPS results.

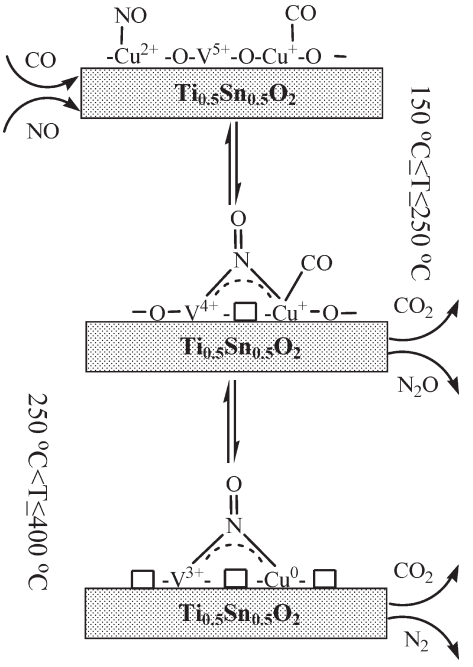

Figure 13. Possible reaction mechanisms for NO reduction by CO over the Cu/V/TS sample below and above 250 °C, □: oxygen vacant site.

Finally, for completion, the mechanism of the NO + CO reaction over Cu/V/TS samples can also be proposed. As shown in Figure 13, when the temperature is below 250 °C, CO and NO molecules mainly interact with Cu^{+} and Cu^{2+} species before reaction. In the meantime, Cu^{2+} and V^{5+} of the sample are reduced by CO to Cu^{+} and V^{4+} ions, respectively. At higher temperatures, adsorption of NO on V^{4+} ions occurs, and the

dx.doi.org/10.1021/cs200045f |ACS Catal. 2011, 1, 468–480

adsorbed NO molecules react with CO molecules that are adsorbed on Cu^+ ions. The reaction is very facile in that temperature region. Simultaneously, the adsorption and reaction leads Cu^+ and V^{4+} to be reduced to Cu^0 and V^{3+}, respectively.

4. CONCLUSIONS

1 For CuO/VO_x/TS catalysts, both copper oxide and vanadium oxide are highly dispersed on TS support at a certain loading amount; for example, ≤ 1.0 mmol Cu/100 m^2 TS and ≤1.2 mmol V/100 m^2 TS. Crystalline CuO and $Cu_2V_2O_7$ are formed when the loading amounts of copper oxide and vanadium oxide are 2.0 mmol Cu/100 m^2 TS and 3.2 mmol V/100 m^2 TS, respectively.

2 There are strong interactions between copper oxide and vanadium oxide, resulting in the formation of V−O−Cu species. As a result, surface dispersed vanadium oxide species reduce more easily when the copper oxide is loaded on the surface of the catalyst. In contrast, the reduction temperature of the dispersed copper oxide species is evidently higher than that without vanadium oxide (CuO/TS catalysts).

3 CuO/VO_x/TS catalysts exhibit better performances toward NO + CO reaction than do CuO/TS catalysts, which should be attributed to the formation of dispersed V−O−Cu species.

4 NO molecules can be adsorbed on Cu^{2+} sites, reduced V^{x+} (V^{4+} or V^{3+}) sites, and TS support, forming −NO and NO_3^- species. However, adsorption of CO molecules proceeds only on Cu^+ sites. All these adsorbates play an important role in the NO + CO reaction. In addition, the reduction of NO by CO over these catalysts goes through different mechanisms at low and high temperatures, which is related to the change in the active species during the reaction. When the temperature is below 250 °C, the main active species are Cu^{2+}/Cu^+ and V^{5+}/V^{4+} couples, but Cu^+/Cu^0 and V^{4+}/V^{3+} couples are the main active species at higher temperatures. .

AUTHOR INFORMATION

Corresponding Author

*(L.D.) Phone: +86-25-83592290. Fax: +86-25-83317761. E-mail: donglin@nju.edu.cn. (F.G.) Phone: +86-25-83596545. Fax: +86-25-83317761. E-mail: gaofei@nju.edu.cn.

ACKNOWLEDGMENT

Financial support from the Project of Jiangsu innovation talent (BK2008001), the National Natural Science Foundation of China (No. 20873060, 20973091), and the National 973 Program of China (No. 2010CB732302) are gratefully acknowledged.

REFERENCES

(1) Martins, R. L.; Baldanza, M. A. S.; Schamal, M. *J. Phys. Chem. B* **2001**, *105*, 10303–10307.

(2) Ozensoy, E.; Hess, C.; Goodman, D. W. *J. Am. Chem. Soc.* **2002**, *124*, 8524–8525.

(3) Hess, C.; Ozensoy, E.; Goodman, D. W. *J. Phys. Chem. B* **2003**, *107*, 2759–2764.

(4) Papavasiliou, J.; Avgouropoulos, G.; Ioannides, T. *Appl. Catal. B: Environ.* **2007**, *69*, 226–234.

(5) Garca, M. F.; Arias, A. M.; Belver, C.; Anderson, J. A.; Conesa, J. C.; Soria, J. *J. Catal.* **2000**, *190*, 387–395.

(6) Yan, W. F.; Chen, B.; Mahurin, S. M.; Schwartz, V.; Mullins, D. R.; Lupini, A. R.; Pennycook, S. J.; Dai, S.; Overbury, S. H. *J. Phys. Chem. B* **2005**, *109*, 10676–10685.

(7) Mirkelamoglu, B.; Karakas, G. *Appl. Catal. A: Gen.* **2006**, *299*, 84–94.

(8) Wang, S. R.; Huang, J.; Zhao, Y. Q.; Wang, S. Q. *J. Mol. Catal. A: Chem.* **2006**, *259*, 245–252.

(9) Shapovalov, V.; Metiu, H. *J. Catal.* **2007**, *245*, 205–214.

(10) Baidya, T.; Marimuthu, A.; Hegde, M. S.; Ravishankar, N.; Madras, G. *J. Phys. Chem. C* **2007**, *111*, 830–839.

(11) Sa, J.; Anderson, J. A. *Appl. Catal. B: Environ.* **2008**, *77*, 409–417.

(12) Wang, C. J.; Zuo, Y. G.; Yang, C. L. *Environ. Eng. Sci.* **2009**, *26*, 1429–1434.

(13) Shelf, M.; Otto, K.; Gandhi, H. T. *J. Catal.* **1968**, *12*, 361–375.

(14) Panayotov, D. *React. Kinet. Catal. Lett.* **1996**, *58*, 73–78.

(15) Panayotov, D.; Khristova, M.; Velikova, M. *Appl. Catal. B: Environ.* **1996**, *9*, 107–132.

(16) Jiang, X. Y.; Ding, G. H.; Lou, L. P.; Chen, Y. X.; Zhang, X. M. *Catal. Today* **2004**, *93−95*, 811–818.

(17) Liu, L. J.; Chen, Y.; Dong, L. H.; Zhu, J.; Wan, H. Q.; Liu, B.; Zhao, B.; Zhu, H. Y.; Sun, K. Q.; Dong, L.; Chen, Y. *Appl. Catal. B: Environ.* **2009**, *90*, 105–114.

(18) Liu, L. J.; Liu, B.; Dong, L. H.; Zhu, J.; Wan, H. Q.; Sun, K. Q.; Zhao, B.; Zhu, H. Y.; Dong, L.; Chen, Y. *Appl. Catal. B: Environ.* **2009**, *90*, 578–586.

(19) Deo, G.; Wachs, I. E.; Haber, J. *Crit. Rev. Surf. Chem.* **1994**, *4*, 141–187.

(20) Miyata, H.; Kohno, M.; Ono, T. *J. Chem. Soc. Faraday Trans. I* **1989**, *85*, 3663–3673.

(21) Reddy, B. M.; Ganesh, I.; Chowdhury, B. *Catal. Today* **1999**, *49*, 115–121.

(22) Wachs, I. E.; Deo, G.; Weckhuysen, B. M.; Andreini, A.; Vuurman, M. A.; Boer, M.; de; Amiridis, M. D. *J. Catal.* **1996**, *161*, 211–221.

(23) Giakoumelou, I.; Fountzoula, C.; Kordulis, C.; Boghosian, S. *J. Catal.* **2006**, *239*, 1–12.

(24) Banas, J.; Najbar, M.; Tomasic, V. *Catal. Today* **2008**, *137*, 267–272.

(25) Huang, J.; Wang, S. R.; Guo, X. Z.; Wang, D.; Zhu, B. L.; Wu, S. H. *Catal. Commun.* **2008**, *9*, 2131–2135.

(26) Li, C.; Zhang, H.; Wang, K. L.; Xin, Q. *Acta Phys.−Chim. Sin.* **1994**, *10*, 33–37.

(27) Kantcheva, M. *Phys. Chem. Chem. Phys.* **2000**, *2*, 3043–3048.

(28) Magg, N.; Giorgi, J. B.; Schroeder, T.; Bäumer, M.; Freund, H. J. *J. Phys. Chem. B* **2002**, *106*, 8756–8761.

(29) Magg, N.; Immaraporn, B.; Giorgi, J. B.; Schroeder, T.; Bäumer, M.; Döbler, J.; Wu, Z. L.; Kondratenko, E.; Cherian, M.; Baerns, M.; Stair, P. C.; Sauer, J.; Freund, H. J. *J. Catal.* **2004**, *226*, 88–100.

(30) Gao, F.; Zhang, Y. H.; Wang, C. L.; Wu, C.; Kong, Y.; Zhao, B.; Dong, L.; Chen, Y. *J. Nanosci. Nanotechnol.* **2007**, *7*, 4508–4514.

(31) Lu, T. C.; Lin, L. B.; Wu, S. Y.; Chen, J.; Zhang, Y. Y. *Nucl. Instrum. Methods Phys. Res., Sect. B* **2002**, *191*, 236–240.

(32) Hansen, J. D.; Boghosian, S. N.; Kustov, A.; Fristrup, P.; Tsilomelekis, G.; Ståhl, K.; Christensen, C. H.; Fehrmann, R. *J. Catal.* **2007**, *251*, 459–473.

(33) Routray, K.; Zhou, W.; Kiely, C. J.; Wachs, I. E. *ACS Catal.* **2011**, *1*, 54–66.

(34) Chary, K. V. R.; Sagar, G. V.; Naresh, D.; Seela, K. K.; Sridhar, B. *J. Phys. Chem. B* **2005**, *109*, 9437–9444.

(35) Sagar, G. V.; Rao, P. V. R.; Srikanth, C. S.; Chary, K. V. R. *J. Phys. Chem. B* **2006**, *110*, 13881–13888.

(36) Srinivas, D.; Hoderich, W. F.; Kujath, S.; Valkenberg, M. H.; Raja, T.; Saikia, L.; Hinzeb, R.; Ramaswamy, V. *J. Catal.* **2008**, *259*, 165–173.

(37) Zhang, X. L.; Klabunde, K. J. *Inog. Chem.* **1992**, *31*, 1706–1709.

(38) Wang, Y. Z.; Zhong, M. Q.; Chen, F.; Yang, J. T. *Appl. Catal. B: Environ.* **2009**, *90*, 249–254.
(39) Ottaviano, L.; Kwoka, M.; Bisti, F.; Parisse, P.; Grossi, V.; Santucci, S.; Szuber, J. *Thin Solid Films* **2009**, *517*, 6161–6169.
(40) Yin, M.; Wu, C. K.; Lou, Y. B.; Burda, C.; Koberstein, J. T.; Zhu, Y. M.; O'Brien, S. *J. Am. Chem. Soc.* **2005**, *127*, 9506–9511.
(41) Ma, H. Z.; Zhuo, Q. F.; Wang, B. *Environ. Sci. Technol.* **2007**, *41*, 7491–7496.
(42) Papavasiliou, J.; Avgouropoulos, G.; Ioannides, T. *J. Catal.* **2007**, *251*, 7–20.
(43) Guo, X. Y.; Bartholomew, C.; Hecker, W.; Baxter, L. L. *Appl. Catal. B: Environ.* **2009**, *92*, 30–40.
(44) Zhao, H. Y.; Bennici, S.; Shen, J. Y.; Auroux, A. *J. Catal.* **2010**, *272*, 176–189.
(45) Mathew, T.; Shiju, N. R.; Sreekumar, K.; Rao, B. S.; Gopinath, C. S. *J. Catal.* **2002**, *210*, 405–417.
(46) Bukallaha, S. B; Bumajdad, A.; Khalil, K. M. S.; Zaki, M. I. *Appl. Surf. Sci.* **2010**, *256*, 6179–6185.
(47) Kornelak, P.; Borzecka-Prokop, B.; Lityńska-Dobrzynska, L.; Wagner, J.; Su, D. S.; Camra, J.; Weselucha-Birczynska, A. *Catal. Today* **2007**, *119*, 204–208.
(48) Banas, J.; Tomasic, V.; Weselucha-Birczynska, A.; Najbar, M. *Catal. Today* **2007**, *119*, 199–203.
(49) Amano, F.; Suzuki, S.; Yamamoto, T.; Tanaka, T. *Appl. Catal. B: Environ.* **2006**, *64*, 282–289.
(50) Li, X. W.; Wan, H. Q.; Liu, B.; Yang, L. J.; Zhu, H. Y.; Chen, H. L.; Zhao, X.; Sun, K. Q.; Dong, L.; Chen, Y. *Catal. Commun.* **2009**, *10*, 741–745.
(51) Kantcheva, M. *Appl. Catal. B: Environ.* **2003**, *42*, 89–109.
(52) Frache, A.; Cadoni, M.; Bisio, C.; Marchese, L. *Langmuir* **2002**, *18*, 6875–6880.
(53) Aylor, A. W.; Larsen, S. C.; Reimer, J. A.; Bell, A. T. *J. Catal.* **1995**, *157*, 592–602.
(54) Busca, G.; Bregani, F.; Forzatti, P. *Appl. Catal.* **1990**, *64*, 259–278.